IIETA International Information and Engineering Technology Association
Advancing the World of Information and Engineering

Traitement du Signal
Vol. 40, No. 2, April, 2023, pp. 501-509
Journal homepage: http://iieta.org/journals/ts

Large-Scale Civil Engineering Structure Deformation Monitoring Research Based on Image Recognition

Xiaodong Yan, Xiaogang Song*

School of Civil & Environmental Engineering and Geography Science, Ningbo University, Ningbo 315211, China

Corresponding Author Email: songxiaogang@nbu.edu.cn

https://doi.org/10.18280/ts.400209

Received: 6 January 2023
Accepted: 11 March 2023

Keywords:
geometric consistency, civil engineering, structural deformation, deformation detection and monitoring

ABSTRACT

Large-scale civil engineering structures may experience deformations during construction and use due to various reasons, affecting the safety and service life of the structures. The application of image recognition technology in the field of civil engineering has promoted the research and development of related technologies, providing new technical means for the monitoring and evaluation of civil engineering structures. Existing image recognition methods may be affected by factors such as lighting, occlusion, and image quality when dealing with large-scale civil engineering structure deformation monitoring, resulting in reduced recognition accuracy. Therefore, this study conducts research on large-scale civil engineering structure deformation monitoring based on image recognition. Traditional civil engineering structure deformation detection methods are presented. A simple and intuitive curve expression is used to describe the deformation characteristics of civil engineering structures, and GCN is used to mine the feature information between adjacent feature points and long-distance related points to improve prediction performance. A graph convolution prediction module and a geometric auxiliary prediction module are set up for the constructed prediction model, and the setting objectives and structural principles of the two modules are explained. In response to the challenges of extracting large-scale civil engineering structure deformation curves, an automatic extraction method based on deep learning networks is proposed, achieving high-precision recognition and extraction of civil engineering structure deformation curves. Experimental results validate the effectiveness of the proposed method.

1. INTRODUCTION

With the continuous development of science and technology, large-scale civil engineering structures (such as bridges, highways, tunnels, dams, etc.) have been widely applied worldwide. However, these engineering structures may experience deformations during construction and use for various reasons, affecting their safety and service life [1-7]. Monitoring structures through image recognition technology can detect potential problems in real-time, helping to determine whether maintenance or reinforcement is needed, thereby prolonging the service life of structures. It can also provide early warning of potential disasters, such as landslides and collapses, providing valuable time for disaster prevention and rescue [8-12]. The application of image recognition technology in the field of civil engineering has promoted the research and development of related technologies, providing new technical means for the monitoring and evaluation of civil engineering structures [13-16]. The use of image recognition technology for civil engineering structure monitoring helps improve engineering management levels, reduce accident risks, and enhance social and economic benefits.

Due to the critical climate conditions of the Qinghai-Tibet Plateau, the surface deformation along highways is difficult to monitor. Yang et al. [17] used sentinel-1A synthetic aperture radar data as a basis and adopts the time series SBAS-InSAR method to evaluate the surface deformation along the Gongyu highway. The results show that the surface deformation in most areas is within the safe range of the highway. In addition, surface deformation shows a strong seasonal effect. Finally, two special points with dangerous surface deformation along the highway are identified. Xu et al. [18] implemented real-time monitoring of existing lines within the impact range of subway structure engineering through a "real-time monitoring system" and inclinometer sensors, providing timely and reliable information for construction units to assess safety during construction and the impact of construction on existing lines, as well as potential hidden dangers or accidents that may jeopardize the safety of construction and existing subway environments. Timely and accurate predictions are made to take effective measures to eliminate hidden dangers and prevent accidents. Ground-based synthetic aperture radar interferometry (GB-InSAR) can continuously monitor regional deformation, enabling near-real-time control of the overall deformation state of dam surfaces. Wang et al. [19] first adopted a multi-threshold strategy and selects coherent point targets using continuous GB-SAR image sequences. A differential GB-InSAR with a CPT-based image subset is developed to solve the dam surface deformation before and after abnormal interruptions. Finally, a deformation monitoring experiment is conducted on a real-life large-scale reservoir dam. The effectiveness and accuracy of the method are verified by comparing the results with the measurements of the inverted monitoring system. Górszczyk and Malicki [20] reported the results of geogrid tests using the Digital Image Correlation (DIC) method and numerical simulations of

laboratory tests on geogrids using the Wide Strip Method. Strain test and analysis results indicate that the DIC method is an effective tool for evaluating the parameters of geogrids used in GRS systems and subgrade structures. In addition to the standard deformation images of the average base, the deformation of any direction and point on the geogrid surface can also be analyzed. The applied measurement method also opens up the possibility of validating multi-model geogrids using the finite element method.

In the existing research findings, the current image recognition methods may suffer from the influence of factors such as illumination, occlusion, and image quality when dealing with large-scale civil engineering structural deformation monitoring. This leads to a decrease in recognition accuracy. When dealing with civil engineering structures in complex environments, existing methods may be affected by natural environments (such as wind, rain, snow, fog, etc.) and human interference (such as vibration, occlusion, equipment failure, etc.), thus reducing the monitoring effect. In response to the shortcomings of these methods, this study conducts research on large-scale civil engineering structural deformation monitoring based on image recognition. The article first introduces traditional civil engineering structural deformation detection methods in section 2. Section 3 uses simple and intuitive curve expressions to describe the deformation characteristics of civil engineering structures, and utilizes GCN to mine feature information between adjacent feature points and distant correlation points, thus improving prediction performance. A graph convolutional prediction module and a geometric auxiliary prediction module are set up for the constructed prediction model, and the setting objectives and structural principles of the two modules are elaborated. Section 4 proposes a deep learning network-based automatic extraction method for the challenges of large-scale civil engineering structural deformation curve extraction, achieving high-precision recognition and extraction of civil engineering structural deformation curves. The experimental results verify the effectiveness of the proposed method.

2. TRADITIONAL CIVIL ENGINEERING STRUCTURAL DEFORMATION DETECTION METHODS

The row coordinate standard deviation method is a basic method for judging the deformation of civil engineering structures. Civil engineering structures (such as bridges, tunnels, dams, etc.) should exhibit certain regularity and continuity in their structural normal vectors under normal conditions. When the structure undergoes deformation, the regularity and continuity of its normal vectors will change. By calculating the standard deviation of the row coordinate data of the normal vectors, the degree of structural deformation can be quantitatively evaluated. Suppose the width of the fine positioning area is represented by q, the standard deviation of the row coordinates is represented by r, and the row coordinate of the j-th column normal vector is represented by $b(j)$. The following formula gives the calculation formula for the standard deviation of the row coordinates:

$$r=\sqrt{\frac{1}{q}\sum_{j=1}^{q}\left(b(j)-\frac{1}{q}\sum_{j=1}^{q}b(j)\right)^2} \tag{1}$$

The row coordinate of the j-th column normal vector can be calculated using the following formula:

$$b(j)=\frac{1}{2}\left(\max\left(S(i,j)\right)+\min\left(S(i,j)\right)\right) \tag{2}$$

Assuming that the pixel value at position (i,j) in the binary image is represented by $s(i,j)$, the height of the fine positioning area is represented by f, and the row coordinate of the point with a pixel value of 1 in the binary image is represented by $s(i,j)$, the calculation formula is as follows:

$$S(i,j)=\begin{cases} i & s(i,j)=1 \\ 0 & s(i,j)=0 \end{cases}, i=1...f \tag{3}$$

3. DEFORMATION MONITORING OF CIVIL ENGINEERING STRUCTURE BASED ON GEOMETRIC CONSISTENCY

To extract more deformation characteristic information of large civil engineering structures and improve the performance of deformation prediction, this study uses simple and intuitive curve expressions to describe the deformation characteristics of civil engineering structures, making deformation modeling easier to understand and implement. With the help of GCN to mine the characteristic information between adjacent feature points and remote associated points, the prediction performance is improved. By introducing the geometric consistency relationship between the position and normal vector of feature points, the prediction method can make full use of the geometric information of feature points, so as to improve the accuracy of prediction results. The positions and normal vectors of feature points are normalized so that feature information of different scales and directions can be processed uniformly. Geometric prediction is also performed according to the geometric relationship between the positions and normal vectors of feature points to further improve the accuracy of normal vector prediction results.

In order to achieve the preset functions, this study sets up a graph convolution prediction module and a geometric auxiliary prediction module for the constructed prediction model. The purpose of setting up the graph convolution prediction module is to fuse the local and non-local information in civil engineering structures to capture the complex relationships in structural deformation characteristics. The main reason is that deformation characteristics of civil engineering structures often contain a large amount of local information (such as the relationship between adjacent feature points) and non-local information (such as the relationship between remote associated points). The use of graph convolutional networks (*GCN*) can effectively fuse this information, enabling the prediction model to capture the deformation characteristics of civil engineering structures more comprehensively and improve the accuracy and reliability of prediction results.

The purpose of setting up the geometric auxiliary prediction module is to explore the inherent geometric relationship between the positions and normal vectors of feature points in order to predict the deformation of civil engineering structures more accurately. Since there is an inherent geometric consistency relationship between the positions and normal vectors of feature points, these relationships can provide valuable information for predicting the deformation of civil

engineering structures. By introducing these geometric relationships, the prediction model can make better use of the geometric information of feature points to improve the accuracy of prediction results. In addition, the geometric auxiliary prediction module can further optimize and improve the accuracy of normal vector prediction results.

In the deformation analysis of large civil engineering structures, feature points are the key elements used to describe the deformation characteristics of structures. Different types of feature points can provide different information to help understand and predict structural deformation. Local neighborhood feature points are usually located in close areas of the structure, reflecting the local deformation characteristics of the structure. Local neighborhood feature points can help us understand the deformation behavior of the structure within a local range, such as cracks, stress concentration areas or local damage. Remote associated feature points are located in areas far apart in the structure, but there may be some association between them. Remote associated feature points help capture the overall deformation characteristics of the structure, such as overall settlement, deformation or distortion. Symmetric feature points: these feature points are located at symmetric positions of the structure. Symmetric feature points can help us understand the deformation characteristics of the structure under the action of symmetric loads. For example, the symmetrical supports of bridges or the symmetrical columns of high-rise buildings.

In order to analyze these different types of feature points and understand the deformation characteristics of large civil engineering structures more comprehensively, this study introduces the self-attention mechanism based on the structure of graph convolution. Figure 1 shows the self-attention mechanism process. The self-attention mechanism can automatically calculate the weight allocation according to the relationship between feature points, not just relying on local neighborhood feature points. This allows the model to better capture the relationship between remote symmetric feature points, providing richer information in deformation prediction. At the same time, the self-attention mechanism can capture long-distance dependencies in the input features, which helps the graph convolution network learn a more comprehensive feature representation. This enables the model to better understand the remote symmetric feature points in civil engineering structures, improving the accuracy of prediction results. Figure 2 shows the graph convolution network structure used.

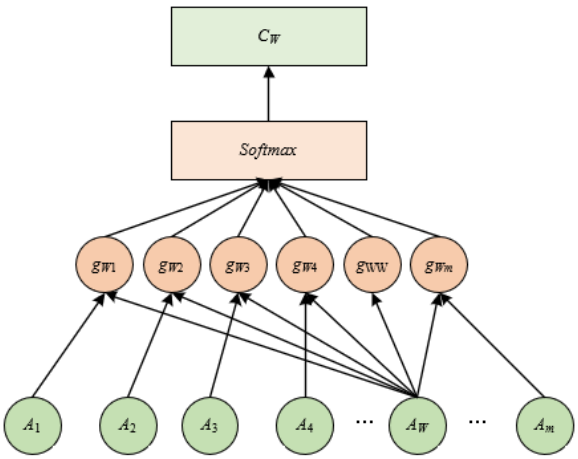

Figure 1. Self-attention mechanism process

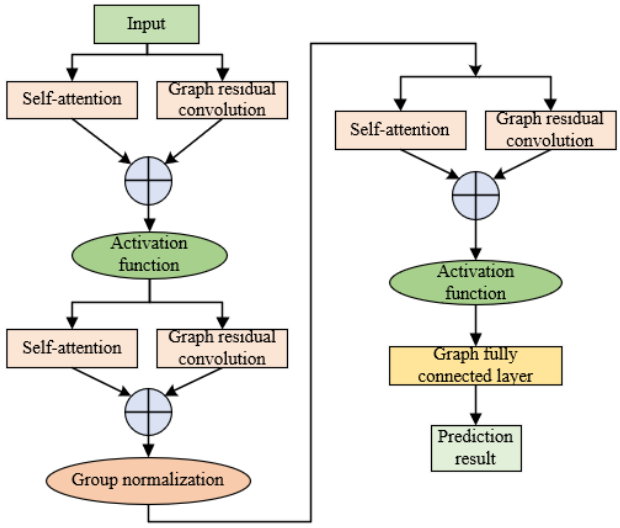

Figure 2. Graph convolution network structure

In order to better deal with the feature information of nonlocal different types of feature points, this study calculates the attention relationship coefficients between different types of feature points based on the attention relationship. Assuming that each feature point contains G-dimensional features, the input of the ith layer of the network is represented by $A_i=\{a_{i1},a_{i2},...,a_{iM}\}$, and the jth node a_{ij} of the ith layer satisfies $a_{ij}\in R^G$, where the number of nodes is M. It can be considered that the input data of the network is an $M\times G$ feature matrix. For each a_{ij}, calculate the attention relationship coefficients with all other nodes, and the calculation formula of the attention relationship coefficients corresponding to node W is as follows:

$$g(a_{iW},a_{ij})=a_{iW}^{T}a_{ij},\ j=1,2,...,M \tag{4}$$

To calculate and compare more conveniently, this study normalizes the calculated attention relationship coefficients based on the *softmax* function. The operation process is as follows:

$$\begin{aligned} X_{Wj} &= soft\max_j\left(g\left(a_{iW},a_{ij}\right)\right) \\ &= \frac{\exp\left(g\left(a_{iW},a_{ij}\right)\right)}{\sum_{v=1}^{M}\exp\left(g\left(a_{iW},a_{iv}\right)\right)} \end{aligned} \tag{5}$$

The calculation results can be used as the weight coefficients between node W and other nodes. Furthermore, the weighted sum of the calculation results can be obtained, which is the deformation feature vector corresponding to node W:

$$C_W=\sum_{j=1}^{M}X_{Wj}a_{ij} \tag{6}$$

There is an inherent geometric consistency relationship between the position and normal vector of the structural deformation feature points. Using this relationship can capture deformation information from different angles, provide more valuable information, and improve the accuracy of deformation prediction. Using this relationship can further

enhance the expressive power of the prediction model. This means that the model can better describe complex deformation behaviors, so as to maintain the integrity of the structure during the prediction process. This will help improve the reliability of deformation prediction for large civil engineering structures.

In order to improve the accuracy of deformation prediction for large civil engineering structures, this study proposes to set up a geometric auxiliary prediction module in the prediction model. First, the position and normal vector estimation of feature points are obtained by the graph convolution deformation prediction network. Then, according to the geometric consistency constraint relationship, the geometric prediction normal vector is calculated by the predicted deformed position. Then, the deformed normal vector predicted by the graph convolution network is fused with the geometric prediction normal vector. Finally, the fused normal vector is input into the graph convolution deformation prediction network again to obtain the final refined deformation prediction result. By introducing the geometric consistency constraint relationship, the model is helped to better capture the geometric relationship between feature points, thus improving the quality of the prediction results. The deformed normal vector predicted by the graph convolution network and the geometric prediction normal vector are fully utilized to obtain a more refined deformation prediction result.

In the module, assuming that each feature point i has n adjacent nodes, the set of adjacent nodes of the feature point (including point i itself) is defined by $M_i = \{(a_n,b_n,c_n)\}$, where the adjacent node of point i is represented by n. Assuming that the points in the neighborhood set centered on point i form a tangent plane, the following equation gives the expression of the set X of neighborhood points:

$$X = \begin{bmatrix} a_1 & b_1 & c_1 \\ \vdots & \vdots & \vdots \\ a_n & b_n & c_n \end{bmatrix} \in R^{n\times 3} \tag{7}$$

Assuming that the constant vector is represented by y and the size of the neighborhood set M_i is represented by n. Because the local feature tangent plane and the normal vector have a mutually perpendicular spatial geometric relationship, the default surface normal vector $m=[m_1,m_2,m_3]$ should meet the linear constraint conditions shown in the following equation:

$$Xm = y, satisfy \ \|m\|_2^2 = 1 \tag{8}$$

Assuming that the vector consisting of all 1's is represented by 1, the minimum solution shown in the following equation can be obtained by solving the above equation based on the least squares method:

$$m = \frac{\left(X^T X\right)^{-1} X^T 1}{\left\|\left(X^T X\right)^{-1} X^T 1\right\|_2} \tag{9}$$

For the feature point i, assuming that the predicted feature point position and the target model point position are represented by ${}_it_i$ and thp_i respectively. Similarly, the normal vector of the feature point is represented by m_i and mhp_i, and the total number of points is represented by l. The total loss function is the sum of the position loss and the normal vector loss of the feature points, that is, $K=q_1*K_{WZ}+q_2*K_{FXL}$. Assuming that the hyperparameters used to balance the contributions between different items are represented by q_1 and q_2, then:

$$K_{WZ} = \sum_{i=1}^{l} \left(t_i - thp_i\right)^2 \tag{10}$$

$$K_{FXL} = \sum_{i=1}^{l} \left(m_i - mhp_i\right)^2 \tag{11}$$

The geometric auxiliary prediction module finally outputs the position estimation and normal vector estimation of the feature points after deformation. The network training method is end-to-end back propagation.

4. EXTRACTION OF DEFORMATION CURVES BASED ON SEGMENTATION NETWORK

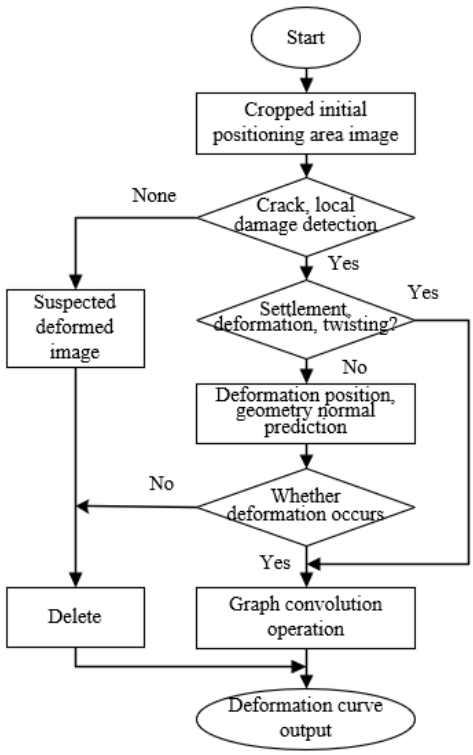

Figure 3. Flow chart of deformation curve extraction algorithm for large civil engineering structures

To accurately identify and extract deformation curves of civil engineering structures, this study proposes an automatic extraction method based on deep learning networks for the challenges of extracting deformation curves of large civil engineering structures. First, the original data is converted and preprocessed so that the deep learning network can learn and predict efficiently. Based on the deformation curves of large civil engineering structures, the specimen is segmented and predicted using the segmentation network optimized in this study. This step divides the specimen into deformed and non-deformed areas. For the deformed labels in the network segmentation results, the deformation curve is optimized and extracted using the edge refinement extraction method to

obtain the final deformation curve extraction result. This method uses sample data-driven deep learning networks to automatically extract deformation curves of specimens, abandoning the complex manual calibration process and greatly improving extraction efficiency. It has high versatility and can be applied to extract different types of deformation curves of large civil engineering structures. Figure 3 shows the flow chart of the deformation curve extraction algorithm for large civil engineering structures.

This study proposes a segmentation prediction network based on *KPconv* to achieve high-quality automatic extraction of deformation curves of large civil engineering structures. By introducing kernel point convolution in the convolutional layer of the network, the features of each feature point can be processed. Kernel point convolution can capture spatial neighborhood information, which helps to better describe the structural features of the feature point data. The network uses an encoder and decoder structure to be responsible for extracting high-level features of the feature point data and generating segmentation results respectively. By adjusting the number of layers in the network model and optimizing network hyperparameters, the performance and generalization ability of the network are further improved.

Define the feature points in the feature point set $T \in R^{M\times 3}$ as a_i, and its corresponding features as $g_i \in G \in R^{M\times C}$. Assuming that the local neighborhood of point a_i is represented by M_a, the local neighborhood can be regarded as a circular neighborhood with point a as the center point and $s \in R$ as the radius, which can be represented by $M_a=\{a_i \in T \| \|a_i-a\| \le s\}$. Based on this, the convolution of the kernel h on the feature point $a \in R^3$ can be defined as:

$$(G*h)(a)=\sum_{a_i \in M_a} h(a_i-a)g_i \tag{12}$$

The key to kernel point convolution is the kernel function h. h takes all adjacent points within the circular neighborhood centered on the feature point a as input. Each neighboring point a_i is centered on $b_i=a_i-a$ to ensure translation invariance. So the domain of h is represented by $Y^3{}_s=\{b \in R^3 \| \|b\| \le s\}$. In order to make the weights of different regions in h different, L kernel points $\{a_l\tilde{} | l<L\} \subset Y^3{}_s$ are defined based on L kernel points, and the related weight matrix mapping features from C_{in} to C_{out} is defined as $\{Q_l | l<L\} \subset R^{Cin\times Cout}$. Assuming the correlation between $a_l\tilde{}$ and b_i is represented by f, the kernel function h for any point $b_i \in Y^3{}_s$ is expressed as:

$$h(b_i)=\sum_{l<L} f(b_i,\tilde{a}_l)Q_l \tag{13}$$

The closer $a_l\tilde{}$ is to b_i, the higher the value of f. Assuming the influence distance of the kernel points is represented by ξ, the linear relationship between them is defined as:

$$f(b_i,\tilde{a}_l)=\max\left(0,1-\frac{\|b_i-\tilde{a}_l\|}{\xi}\right) \tag{14}$$

In order to significantly improve the detail performance of the boundary area in the segmentation result and make it smoother and more refined, this study proposes a method of using conditional random fields (*CRF*) to optimize local details. Conditional random field (*CRF*) is a probabilistic graph model that can transmit spatial information of segmentation results by utilizing the correlation between points. By considering the interdependence between adjacent points, spatial information is transmitted to the segmentation results, thereby optimizing local details. *CRF* makes full use of the correlation between points to achieve effective transmission of spatial information. Its processing can make up for possible deficiencies in the prediction results of the segmentation network, and obtain a more accurate and robust deformation curve extraction results.

Assuming that the normal vector corresponding to the i-th point in the prediction result feature point $E \in R^{M\times G}$ of the segmentation network is represented by m_i, the predicted label value is represented by r_i, the number of nodes in the point cloud is represented by M, and the feature dimension contained in each point is represented by G. The unary potential function is represented by $\mu_v(r_i)=-log(H(r_i))$, and the segmentation label prediction probability of each point is represented by $H(r_i)$, then:

$$O(r)=\sum_i \mu_v(r_i)+\sum_{i<j}\mu_{ij}(r_i,r_j),\ j=1,2,...,M \tag{15}$$

Let $j \in [1, M]$, the label compatibility function is represented by $\lambda(r_i,r_j)$, the Gaussian function weight is represented by θ_i, and the Gaussian function with a standard deviation of ω_i is represented by $q_{\omega i}$. The following equation defines the binary potential function $\mu_{ij}(r_i,r_j)$:

$$\mu_{ij}(r_i,r_j)=v(r_i,r_j)\begin{pmatrix}\theta_1 q_{\omega 1}\|H_i-H_j\| \\ +\theta_2 q_{\omega 2}\|H_i-H_j\|\|m_i-m_j\|\end{pmatrix} \tag{16}$$

Furthermore, the location of the rotation center point is determined by the x-axis and y-axis coordinates of the center point of the deformed label part obtained by prediction and the minimum z-axis coordinate of all points in the deformed label part obtained by prediction. Choose the point with the minimum z-axis in the deformed label part obtained by prediction as the starting point of rotation and the first deformation curve feature point. Rotate the starting point of rotation counterclockwise around the rotation center point by 1°. Choose the point closest to the point after rotating 1° as the second deformation curve feature point. Take the point rotated 1° in the previous step as the new starting point of rotation. Repeat steps 3-5, continue to rotate counterclockwise by 1°, and choose the point closest to the rotated point as the next deformation curve feature point. Repeat this process until the curve extraction of the entire deformed area is completed. By this method, deformation curve extraction can be performed on the deformed label part after boundary refinement of the segmentation result, so as to achieve high-quality automatic extraction of deformation curves of civil engineering structures.

In order to achieve uniform distribution of feature points on the deformation curve. First, the interpolation operation makes the curve smoother and fills the gaps between the curves. Then, equal angular sampling ensures that the angle between feature points is basically equal, so that the feature points are uniformly distributed on the deformation curve. Finally, by repeating the sampling process, a refined deformation curve extraction result with 360 feature points can be obtained.

5. EXPERIMENTAL RESULTS AND ANALYSIS

Figure 4 shows the network model training results. The results show that the proposed network model performs well on the training set, with an accuracy of 72.89% and a *Kappa* coefficient of 0.6381. On the validation set, the accuracy is 69.43% and the *Kappa* coefficient is 0.5405. Although the accuracy and *Kappa* coefficient on the validation set are slightly lower than those on the training set, this can be attributed to the smaller amount of validation set data, which may not fully represent the complexity of the problem. However, the accuracy and *Kappa* coefficient on the validation set are still in the moderate consistency classification range, which means that the model has a certain generalization ability. Combined with the previous questions and answers, the method proposed in this study is effective and advanced in extracting deformation curves of large civil engineering structures. By using deep learning methods and an optimized network structure, the model can automatically extract deformation curves and optimize the results, thereby improving analysis efficiency and accuracy.

Table 1 shows the distance between feature points of the specimen marker block. Based on the above table, an error analysis of the distance between the feature points of the specimen marker block is performed. First, calculate the average value of the distance between the marker block feature points in each stage. Then, calculate the percentage error of the average value in each stage relative to the corresponding distance. Finally, draw conclusions. The average values in each stage are as follows:

- Stage 1: (340.69 +33971+353.84+352.57+ 359.01+ 359.51+368.51+368.51+ 367.44)/ 9≈355.31
- Stage 2: (406.04+391.24+401.61+ 391.41+392.59+ 399.64+405.51+ 398.64+ 392.61)/9≈397.54
- Stage 3: (445.61+440.61+437.15+439.91+433.81+ 440.61+436.91+431.51 +436.27)/ 9≈436.82

Continue to calculate the percentage error in each stage:

- Stage 1 percentage error: |(340.69-355.31)/355.31| =4.12%;
- Stage 2 percentage error: |(406.04-397.54)/397.54| =2.14%;
- Stage 3 percentage error: |(445.61-436.82)/436.82| =2.01%.

According to the error analysis, we can see that in each stage, the percentage error of the distance between the marker block feature points is relatively small. This shows that the deformation monitoring of large civil engineering structures has a certain accuracy in the experiment using civil engineering structure deformation.

In order to better extract the edge curve of the deformation area of the civil engineering structure and enhance the details of the low gray value part of the deformation area of the civil engineering structure, preparing for the subsequent deformation defect detection and recognition. This study selects the method of median filtering combined with logarithmic transformation to process the region precisely positioned by row and column coordinates. Figure 5 shows the precise positioning results of the deformation curve. For the extraction of the edge curve of the deformation region, the experimental results show that the civil engineering structure deformation curve after processing is clearer and more continuous, which is helpful for subsequent deformation recognition. The processed image has higher contrast and richer detail information in the low gray value area, which verifies the effectiveness of the model in the application of identifying civil engineering structure deformation.

Table 2 shows the specimen deformation simulation test change and actual change data. Based on the above table, an error analysis of the specimen deformation simulation test change and actual change data is performed to calculate the percentage error between the deformation test value and the actual value in each stage.

The percentage error in stage 1 is as follows:
(1) |(3.515-3.471)/3.471|=1.27%;
(2) |(3.941-3.412)/3.412|=15.48%;
(3) |(1.745- 1.810)/ 1.810| =3.59%;
(4) |(2.815-2.811)/2.811|=0.14%;
(5) |(2.741-2.610)/2.610| =5.02%;
(6) |(2.845-2.730)/2.730|= 4.21%;
(7) |(2.924-2.964) /2.964|=1.35%;
(8) |(2.110 -2144)/2.144| =1.59%;
(9) |(1.841-2.110)/2.110|=12.75%

The percentage error in stage 2 is as follows:
(1) |(3.155-3.120)/3.120|= 1.12%;
(2) |(4.101-4.151)/4.151|= 1.20%;
(3) |(2.851-2.614)/2.614| =9.07%;
(4) |(3.415-3.512)/3.512|=2.76%;
(5) |(2.515-2.851)/2.851|=11.79%;
(6) |(3.154-3.211)/3.211|= 1.78%;
(7) |(1.615-1.914)/1.914|= 15.61%;
(8) |(2.614- 2.641)/2.641|= 1.02%;
(9) |(2.815- 2.684)/2.684|=4.88%

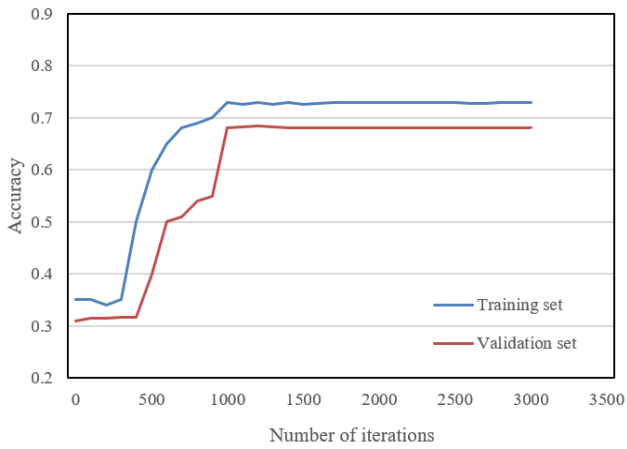

Figure 4. Network model training results

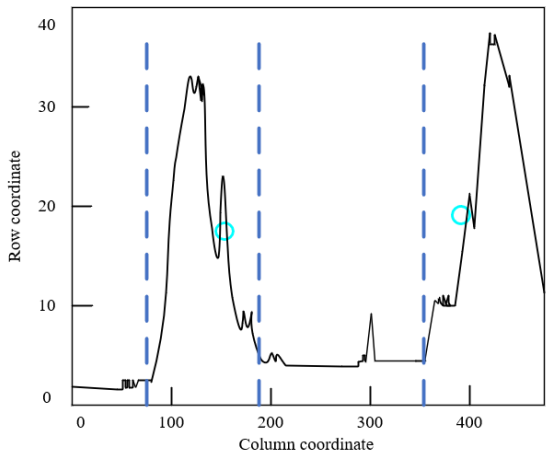

Figure 5. Precise positioning of deformation curves

Table 1. Distance between feature points of specimen marker block

Horizontal distance from shooting point (cm)	Distance between feature points of marker block in stage 1 (mm)	Distance between feature points of marker block in stage 2 (mm)	Distance between feature points of marker block in stage 3 (mm)
112	340.69	406.04	445.61
158	339.71	391.24	440.61
204	353.84	401.61	437.15
250	352.57	391.41	439.91
296	359.01	392.59	433.81
342	359.51	399.64	440.61
388	368.51	405.51	436.91
434	368.51	398.64	431.51
480	367.44	392.61	436.27

Table 2. Specimen deformation simulation test change and actual change data

Stage 1 deformation test value (mm)	Stage 1 actual deformation value (mm)	Stage 2 deformation test value (mm)	Stage 2 actual deformation value (mm)
3.515	3.471	3.155	3.120
3.941	3.412	4.101	4.151
1.745	1.810	2.851	2.614
2.815	2.811	3.415	3.512
2.741	2.610	2.515	2.851
2.845	2.730	3.154	3.211
2.924	2.964	1.615	1.914
2.110	2.144	2.614	2.641
1.841	2.110	2.815	2.684

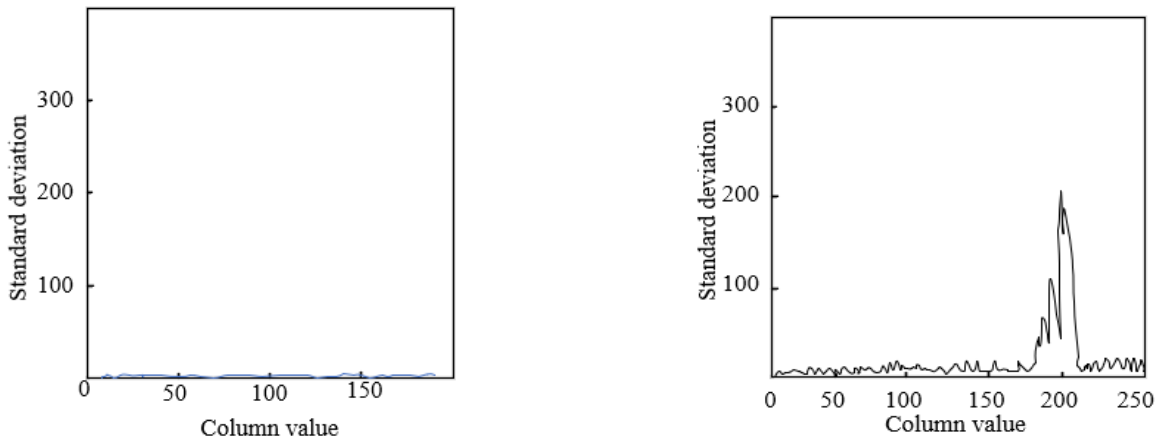

Figure 6. Local column standard deviation

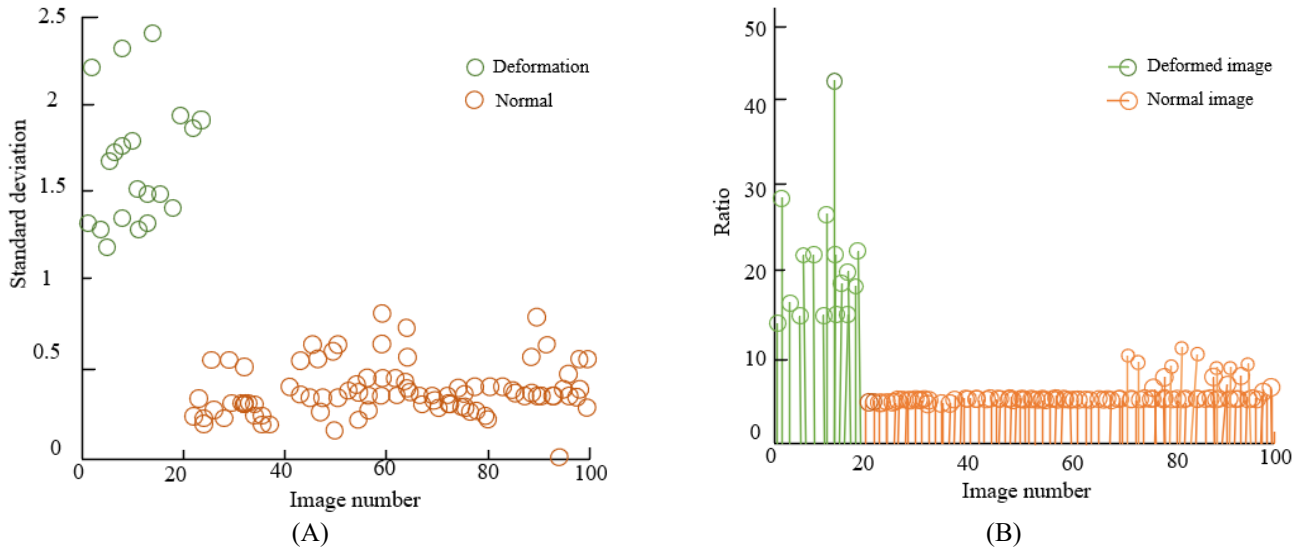

Figure 7. Calculation result statistics

According to the error analysis, we can see that in each stage, there is a certain fluctuation in the percentage error between the deformation test value and the actual value, but most of the errors are small. This shows that the simulation test results have a certain accuracy in the experiment.

Figure 6 shows the calculation result of the ratio of the maximum value of the standard deviation of the sum of the local column gray values of the image of the deformation area of the civil engineering structure to the mean value. As can be seen from the figure, for different deformation areas of civil engineering structures, the ratio of the maximum value of the standard deviation of the sum of the local column gray values to the mean value may be significantly higher in the deformation defect area than in other areas. By comparing the ratio of different areas, the specific location of deformation defects can be determined, indicating that the model constructed in this study can effectively detect and identify deformation defects in civil engineering structures. These experimental results verify the effectiveness of the model and indicate that the method has practical value in identifying deformation defects in civil engineering structures.

In summary of the previous analysis conclusions, we can summarize the accuracy of the algorithm:

(1) For the error analysis of the distance between feature points, we found that the error is relatively small, proving that the algorithm has a certain accuracy in estimating the distance between feature points.

(2) For the error analysis of the specimen deformation simulation test change and the actual change data, the results show that the error is small, which means that the algorithm has good performance in the simulation deformation test.

In order to more accurately identify the deformation state of civil engineering structures, take 20 images of deformed civil engineering structures and 80 images of normal civil engineering structures to calculate the standard deviation of the marker block feature points and statistics the distribution of standard deviations. Similarly, take 20 images of deformed civil engineering structures and 80 images of normal civil engineering structures to calculate the distribution of K values. Figure 7 shows the calculation result statistics. As can be seen from the figure, for the standard deviation of marker block feature points, the distribution of deformed images and normal images may be significantly different. The standard deviation of deformed images may be relatively large, while the standard deviation of normal images may be relatively small. For the K value distribution, the distribution of deformed images and normal images may also be significantly different. The K value of deformed images may be higher, while the K value of normal images may be lower. It can be seen that the distribution of standard deviation and K value of marker block feature points shows obvious differences between deformed images and normal images. These experimental results further verify the effectiveness of the model and indicate that the method has practical value in identifying the deformation state of civil engineering structures.

6. CONCLUSION

This study conducts research on deformation monitoring of large civil engineering structures based on image recognition. The traditional methods for finding deformation of civil engineering structures are given. Simple and intuitive curve expressions are used to describe the deformation characteristics of civil engineering structures. With the help of GCN, the feature information between adjacent feature points and distant related points is mined to improve the prediction performance. A graph convolution prediction module and a geometry-assisted prediction module are set up for the constructed prediction model, and the setting objectives and structural principles of the two modules are explained. In view of the challenges of extracting deformation curves of large civil engineering structures, an automatic extraction method based on deep learning networks is proposed to achieve high-precision identification and extraction of deformation curves of civil engineering structures. The network model training results are given to verify that the constructed model can automatically extract deformation curves and optimize the results, thereby improving analysis efficiency and accuracy. The distance between feature points of the specimen marker block and the precise positioning results of the deformation curve are given to verify the effectiveness of the model in this study in identifying civil engineering structure deformation applications. The specimen deformation simulation test change and actual change data and the calculation result of the ratio of the maximum value of the standard deviation of the sum of the local column gray values of the image in the deformation area of the civil engineering structure to the mean value are given to further verify the effectiveness of the model and indicate that the method has practical value in identifying deformation defects in civil engineering structures.

REFERENCES

[1] Wang, Y., Furkan, M.O., Bartoli, I., Lu, F. (2022). Power self-sustained wireless bridge deformation monitoring system based on solar photovoltaic. IEEE Journal of Emerging and Selected Topics in Industrial Electronics, 4(1): 87-96. https://doi.org/10.1109/JESTIE.2022.3204487

[2] Xu, X., Yuan, Y., Zhang, T., Li, K., Wang, S., Liang, C., Zhu, H. (2022). A silanized MCNT/TPU-based flexible strain sensor with high stretchability for deformation monitoring of elastomeric isolators for bridges. Construction and Building Materials, 338: 127664. https://doi.org/10.1016/j.conbuildmat.2022.127664

[3] Zhao, L., Yang, Y., Xiang, Z., Zhang, S., Li, X., Wang, X., Chen, M. (2022). A novel low-cost GNSS solution for the real-time deformation monitoring of cable saddle pushing: A case study of guojiatuo suspension bridge. Remote Sensing, 14(20): 5174. https://doi.org/10.3390/rs14205174

[4] Vorwagner, A., Schlögl, M., Widhalm, B., Avian, M., Prammer, D., Leopold, P., Honeger, C. (2021). Contactless deformation detection for bridge monitoring: First application of Sentinel-1 radar data in Austria. In Bridge Maintenance, Safety, Management, Life-Cycle Sustainability and Innovations, Nanjing, China, pp. 208-214.

[5] Shan, W., Wang, C.J., Hu, Q. (2012). Expressway and road area deformation monitoring research based on InSAR technology in isolated permafrost area. In 2012 2nd International Conference on Remote Sensing, Environment and Transportation Engineering, pp. 1-5. https://doi.org/10.1109/RSETE.2012.6260574

[6] Rui, Y.Q., Chen, J.Y., Ding, X. (2010). On the deformation monitoring based on integrating InSAR with

GPS for expressway/goaf. Dongbei Daxue Xuebao/Journal of Northeastern University, 31(12): 1773-1776.
[7] Anderegg, P., Bronnimann, R., Raab, C., Partl, M. (2002). Long-term health monitoring of pavement deformations on an expressway. VDI BERICHTE, 1685: 141-146.
[8] Luo, T. (2021). Bridge deformation monitoring based on high precision beidou positioning. In 2020 International Conference on Applications and Techniques in Cyber Intelligence: (ATCI 2020), pp. 1086-1091. https://doi.org/10.1007/978-3-030-53980-1_164
[9] Zhou, G.D., Liu, D.K. (2021). Deformation features of a long-span arch bridge based on long-term monitoring data. In Bridge Maintenance, Safety, Management, Life-Cycle Sustainability and Innovations, pp. 2279-2284.
[10] Nguyen, T.L., Nguyen, H.H. (2021). Application of artificial neural network for recovering GPS—RTK data in the monitoring of cable-stayed bridge deformation. In Structural Health Monitoring and Engineering Structures: Select Proceedings of SHM&ES 2020, 148: 63-75. https://doi.org/10.1007/978-981-16-0945-9_5
[11] Fan, H.D., Deng, K.Z., Zhu, C.G., Chen, B.Q., Li, P.X. (2012). Deformation monitoring and prediction methods for expressway above goaf based on time series SAR technique. Journal of China Coal Society, 37(11): 1841-1846.
[12] Zhang, L., Cui, Y., Shi, B. (2021). Complex deformation monitoring of shield tunnel segment joints using distributed fiber optic sensing technology: Experimental verification. IEEE Sensors Journal, 22(4): 3236-3245. https://doi.org/10.1109/JSEN.2021.3139697
[13] Zhang, J.W., Yuan, K., Mao, J.J., Liu, J. (2022). Research on abnormal identification method of deformation monitoring data in tunnel construction. Conference Proceedings of the 10th International Symposium on Project Management, China, ISPM 2022, 1039-1048.
[14] Wang, T., Tang, Y., Yang, H., Xu, X., Liu, W., Li, X. (2022). Convergence deformation monitoring of a shield tunnel based on flexible long-gauge FBG sensors. Mechanics of Advanced Materials and Structures, 29(19): 2827-2835. https://doi.org/10.1080/15376494.2021.1879328
[15] Sui, Y., Cheng, X.H., Li, G.Y., Pu, L.J., Li, C.D., Liao, P.Y. (2022). Inversion analysis of deformation and force of shield tunnel segments based on distributed optical-fibre monitoring. Gongcheng Lixue/Engineering Mechanics, 39(S): 158-163. https://doi.org/10.6052/j.issn.1000-4750.2021.06.S031
[16] Yang, H., Xu, X. (2021). Structure monitoring and deformation analysis of tunnel structure. Composite Structures, 276: 114565. https://doi.org/10.1016/j.compstruct.2021.114565
[17] Yang, Y., Sun, Y., Wu, S., Dong, X., Huang, H., Cao, X., Meng, Z. (2021). Surface deformation monitoring of a section of gongyu expressway based on SBAS-InSAR technology. In E3S Web of Conferences, 233: 01149. https://doi.org/10.1051/e3sconf/202123301149
[18] Xu, Y., Li, Y., Qiu, J. (2022). Application of inclination sensor in real-time remote monitoring system of tunnel structure deformation. Wireless Communications and Mobile Computing, 2022: Article ID 8079543. https://doi.org/10.1155/2022/8079543
[19] Wang, P., Xing, C., Pan, X. (2020). Reservoir dam surface deformation monitoring by differential GB-InSAR based on image subsets. Sensors, 20(2): 396. https://doi.org/10.3390/s20020396
[20] Górszczyk, J., Malicki, K. (2019). Digital image correlation method in monitoring deformation during geogrid testing. Fibres & Textiles in Eastern Europe. 27(2): 84-90. https://doi.org/10.5604/01.3001.0012.9992